A comparative study on the performance of inert and functionalized spheres coated with solid dispersions made of two structurally related antifungal drugs

Naila A. Mugheirbi[1,2], Peter O'Connell[1], Dolores R. Serrano[1], Anne Marie Healy[1], Lynne S. Taylor[2] and Lidia Tajber[1]*

[1] School of Pharmacy and Pharmaceutical Sciences, Trinity College Dublin, College Green, Dublin 2, Ireland.

[2] Department of Industrial and Physical Pharmacy, College of Pharmacy, Purdue University, West Lafayette, Indiana, 47907, USA.

*corresponding author Lidia Tajber, School of Pharmacy and Pharmaceutical Sciences, Trinity College Dublin, College Green, Dublin 2, Ireland. Tel: +35318962787. Email: ltajber@tcd.ie.

Abstract

Fluid bed coating offers potential advantages as a formulation platform for amorphous solid dispersions (ASDs) of poorly soluble drugs, being a one-step manufacturing process which could reduce the risk of phase separation associated with multiple step manufacturing approaches. However, the impact of the physicochemical nature of nonpareil carriers on the properties and drug release from the ASDs has not been studied in detail. In this work, tartaric acid (TAP) and microcrystalline cellulose (CEL) spheres were chosen as examples of functional and inert beads, respectively. Two structurally related triazole antifungals, itraconazole (ITR) and posaconazole (POS), were chosen as model drugs. Solid-state investigations revealed that the fluidized bed process result in both types of spheres uniformly coated with ITR and POS ASDs based on Eudragit® L100-55 (EUD). A single glass transition temperature (T_g) was determined for each of the ASDs. Infrared studies suggested the presence of a weak interaction between POS and TAP, which translated into premature release of POS from the POS/EUD ASD coated TAP spheres in FaSSGF and subsequently lower POS cumulative release in comparison to the ASD coated on CEL beads. High resolution investigations of morphological and compositional changes during dissolution, using scanning electron microscopy and atomic force microscopy coupled with nanoscale thermal investigation, revealed that crystallization of the drug from the ASDs was induced during dissolution when TAP spheres were used as carriers. In contrast, ASDs coated on CEL underwent phase separation and drug-rich nanospecies were formed in the matrix due to the solubility gap between the drug and EUD in FaSSIF. This study demonstrates that properties of carrier for the ASD fundamentally affect the drug release properties and the proper selection of nonpareil beads is critical to ensure product quality.

Keywords: itraconazole, posaconazole, solid dispersion, phase separation, fluid bed coating

Introduction

Solid oral drug delivery systems can be generally classified into two main groups: single unit (SU) dosage forms, such as tablets, and multiple unit (MU) dosage forms, such as pellets, spheres, granules, and microparticles. MU dosage forms offer several advantages over SU formulations including superior distribution along the gastrointestinal tract, which could improve the bioavailability and reduce the risk of premature drug release in the stomach from controlled release formulations[1,2]. MU dosage forms can be administered as filled capsules or compressed tablets. Ideally, the compressed multi-particulates should disintegrate rapidly, at the desired site, and compaction should exert minimal effects on the mechanical properties and performance of the original pellets[1,3].

A promising applications of MU formulations is the administration of drug-polymer amorphous solid dispersions (ASDs)[1,4]. This is usually accomplished via depositing the ASD onto spheres or pellets, referred to as carriers, using a fluid bed coating technique. The formulation of poorly soluble active pharmaceutical ingredients (APIs) into ASDs is a promising platform to improve their apparent solubility and consequently bioavailability[5]. This improvement is due to the high-energy state of amorphous forms relative to their crystalline counterparts because of the disrupted crystal lattice. To stabilize the amorphous state, the API must be molecularly dispersed into an amorphous polymer to form a one-phase system and hence avoid crystallization. Thus, preventing phase separation into drug-rich and polymer-rich domains within the ASD is of utmost importance to achieve the solubility advantage. Usually, polymers forming ASDs possess a relatively high glass transition temperature (T_g) when compared to the pure amorphous drug, which subsequently results in lower API molecular mobility and crystallization tendency[6]. In addition, the polymer is expected to protect the drug in the ASD from crystallization during dissolution. If phase separation

occurs during ASD dissolution, the polymer-rich phase will dissolve quickly, leaving behind the drug-rich phase, which will have poorer wettability and inferior dissolution performance[7].

Although considerable attention has been focused on spray drying and hot melt extrusion to manufacture ASDs, fluid bed coating offers potential advantages. Fluid bed coating can be considered as a one-step manufacturing process with no additional milling, drying or mixing steps required, which reduces the risk of phase separation in an ASD[4]. The carrier on which the ASD is deposited, can be neutral (inert), e.g. microcrystalline cellulose and sugars, or functional, such as tartaric acid. Sugar spheres, or so-called nonpareil seeds, are the most commonly explored category of materials and have been successfully used to formulate the marketed oral dosage form of itraconazole, Sporanox®[8].

Itraconazole (ITR) belongs to the family of weakly basic triazole antifungals and exhibits pH-dependent solubility with an absolute bioavailability of 30% for the marketed product Sporanox®[9]. It has been extensively studied as a model drug to address solubility and dissolution issues associated with the Biopharmaceutics Classification System (BSC) class II APIs. Examples of manipulations with the solid-state properties of ITR include formulation as ASDs, crystal habit alteration, co-crystal formation and nanosization[8,10]. Posaconazole (POS) is a second-generation triazole antifungal with an extended spectrum of antifungal activity compared to ITR[11]. POS is structurally similar to ITR with a fluorine atom and a furan ring replacing the chlorine and dioxolane moieties in ITR[12], as shown in Figure 1. Despite the relatively higher solubility and extended therapeutic spectrum of POS compared to ITR, the use of POS is limited to immune-compromised patients due to the high cost and low bioavailability of the marketed product Noxafil®. Noxafil®, an ASD of POS with HPMCAS, was marketed recently and it is the only solid oral dosage form available for POS[12]. ASDs of the aforementioned azole antifungals, especially

ITR, have been widely investigated and although ITR is commercially available as a pellet based formulation, the impact of the nature of the pellets used in the formulation on the biopharmaceutical performance of those drugs has not been studied. In general, information on how the characteristics of the carrier affect the formulation and performance of ASDs is fragmentary. Therefore the goal of this study was to investigate the impact of physicochemical properties of the carrier on a range of ASD properties using ITR and POS as model drugs. To this end, inert spheres of microcrystalline cellulose and functional spheres of tartaric acid were chosen. An enteric polymer, poly(methacrylic acid-co-ethyl acrylate) (as Eudragit® L100-55), was used as both drugs are absorbed in the small intestine. ASDs were coated onto the spheres using fluid bed coating and the coated spheres were characterized using various techniques. Finally, the dissolution performance of those spheres along with morphological changes during dissolution was investigated using high resolution techniques including Scanning Electron Microscopy (SEM) and Atomic Force Microscopy (AFM).

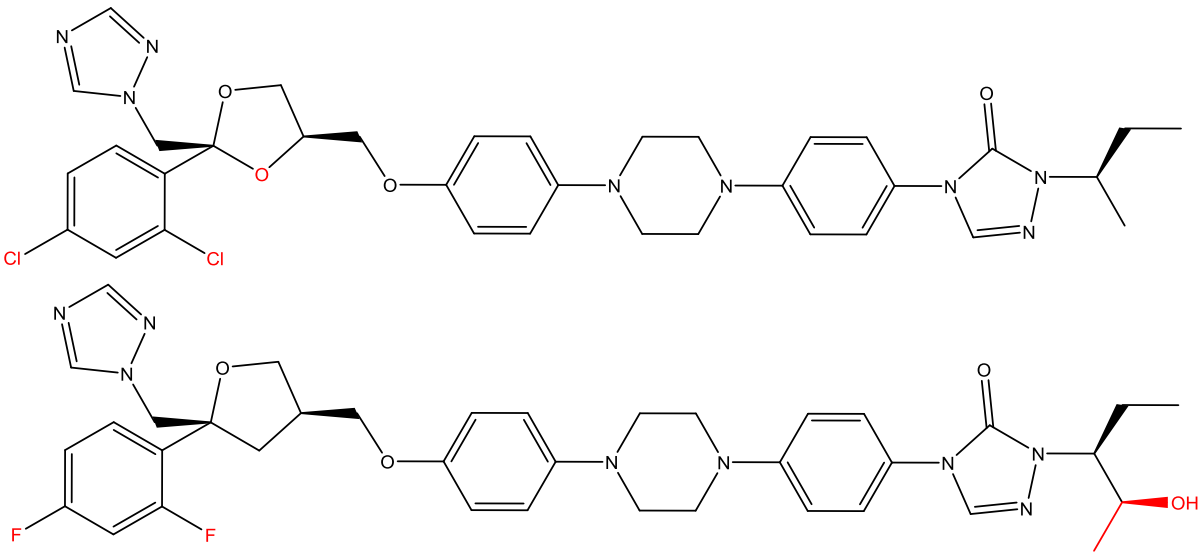

Figure 1. Chemical structures of ITR (top) and POS (bottom) with structural differences between the two compounds highlighted in red.

Materials and Methods

Materials

ITR was a gift from Neuland Laboratories Ltd. (Welding, Hamburg, Germany). POS was purchased from Kemprotec Ltd. (Samilthorn, UK). Tartaric acid (TAP®, subsequently referred to as TAP) and microcrystalline cellulose (Cellets®, subsequently referred to as CEL) beads were kindly donated by Pharmatrans Sanaq AG (Allschwil, Switzerland). The mean bead size was 425 µm (supplier specifications) for both TAP and CEL formulations. Eudragit® L100-55 (EUD) was purchased from Evonik Röhm GmbH (Darmstadt, Germany). Absolute ethanol Chromasolv® and dichloromethane (DCM) (HPLC grades) were purchased from Sigma-Aldrich (Dorset, UK). Acetonitrile HPLC grade was purchase from Fisher scientific (Loughborough, UK). Water (≥99.8%), employed in DVS experiments, was purchased from Sigma-Aldrich (Dorset, UK).

Methods

Fluidized Bed Coating

A quantity of 3 g drug-polymer mixture (1:2 w/w drug:EUD) was completely dissolved in 100 ml of 35:65 v/v ethanol/DCM mixture. The solution was coated onto 7 g of each bead type using a Mini-Glatt fluidized bed dryer (Glatt Ingenieurtechnik GmbH, Germany) under the following operating parameters: inlet gas temperature 40 °C, nitrogen flow rate 25 m^3/h, atomizing gas pressure 1 bar, coating feed rate 0.5 ml/min. When the spraying had finished, the beads were left to dry for 15 min in the chamber under a nitrogen gas purge. The collected spheres were further dried for 12 hr in an oven (Memmert, Schwabach, Germany) at 40 °C.

Powder X-ray Diffraction (PXRD)

PXRD measurements were performed using a Rigaku Miniflex II, desktop X-ray diffractometer (Japan) equipped with a Cu Kα radiation X-ray source. The spheres were tightly packed on a

double sided tape mounted on a low-background silicon sample holder and scanned over a 2θ range of 5–40° [8].

Modulated Temperature Differential Scanning Calorimetry (mDSC)

Thermal behavior of the ASDs coated on the spheres was analyzed using a DSC Q200 (TA Instruments, UK). Approximately 12 mg intact (non-crushed) spheres were placed in a crimped T_{zero} aluminum pan and heated from 25 to 200 °C using a 5 °C/min heating rate, ±0.796 modulation amplitude and 60 s modulation period. The data were analyzed using Universal Analysis® (version 4.7A) software. A baseline run was performed for each sample to minimize sample holder mass error.

Size Measurement

Measurements of size and size distributions of TAP and CEL spheres before and after coating with ASDs were performed using a laser diffraction particle size analyzer Mastersizer 2000 (Malvern instruments Ltd., Malvern, UK). A Scirocco dry feeder instrument (Malvern instruments Ltd., Malvern, UK), operating with 2 bar pressure, was used to disperse the spheres for analysis. An obscuration rate of 0.5-6% was obtained under a vibration feed rate of 50%.

Scanning Electron Microscopy

A Zeiss Supra variable Pressure Field Emission Scanning Electron Microscope (Germany) equipped with a secondary electron detector and accelerating voltage of 5 kV was used for the morphological examination of the spheres before and after coating. In addition, the instrument was also used to investigate the microscopic transformation of the material during dissolution. Samples were fixed on aluminum stubs using carbon tabs. All samples were sputter-coated with a layer of gold/palladium under vacuum before analysis.

Dynamic Vapor Sorption and Time-lapse Imaging of Morphological Changes

Moisture sorption profiles of each sample were determined using a DVS Advantage-1 automated gravimetric vapor sorption analyzer (Surface Measurement Systems Ltd., London, UK). Samples were equilibrated at 0% RH until dry ($dm/dt \leq 0.002$ mg/min for at least 10 min) and the reference mass was recorded. Each sample was exposed to a relative humidity ramp from 0% to 90% and back to 0% with 10% steps at 25±0.1 °C. Photographs were captured by the end of every step during the course of sorption and desorption cycles using the built-in video camera (x100) to visualize the spheres' transformations in real-time.

Solid State Fourier Transform Infrared Spectroscopy (FTIR)

FTIR was performed on a Spectrum One FT-IR Spectrometer (Perkin Elmer, Connecticut, USA) equipped with Spectrum Software version 6.1. A spectral range of 650-4000 cm^{-1} with a resolution of 4 cm^{-1}, scan number of 10 and scan speed of 0.2 cm/s were employed. KBr disks, with a sample loading of 1%, were produced by direct compression under a pressure of approximately 10 bar for 1 minute. Disordered forms of pure drug samples were produced via milling of the crystalline drug for 2 hr at room temperature using a Retsch® planetary ball mill PM 100 (Haan, Germany). Milling was performed in intervals of 10 minutes with 10 minute breaks in between the processing stages. Drug/polymer ASDs were produced via solvent evaporation from ethanol:DCM (35:65 v/v) using a Rotavapor® (model R-205, Buchi, Flawil, Switzerland) at 250 mbar pressure and temperature of 35 °C. PXRD was performed on the milled samples and the materials made by solvent evaporation (Figure SI.1).

Determination of Drug Content

HPLC was used to quantify the amount of drug in the spheres. In these experiments, 10 spheres (around 1 mg) were dissolved in 1.5 mL of the mobile phase and analyzed using an Alliance HPLC

with a Waters 2695 separations module system and Waters 2996 photodiode array detector. The mobile phase consisted of 40:60 (v/v) phosphate buffer (pH=6.8):acetonitrile for ITR and 40:60 (v/v) water:acetonitrile for POS. The mobile phase was filtered through a 0.45 µm membrane filter (Pall Supor® 0.45 µm, 47 mm diameter) before use. Separation was performed on a Waters Symmetry® C18 5 µm (4.6*150 mm) column at a UV detection wavelength of 260 nm with an injection volume of 50 µL. The elution was carried out isocratically at ambient temperature with a flow rate of 1 mL/min. Empower® software was used for peak evaluation. The calibration curves were linear for both components between 0.05 - 50 µg/mL ($R^2 > 0.9999$).

Surface Area Measurements

Bulk surface area (T_{BET}) of the "as received" spheres was determined by Brunauer, Emmett, Teller (BET) isotherm using a Micromeritics Gemini VI (USA) surface area analyzer. A quantity of 3 g of each types of spheres (CEL or TAP) were used for the study. The mean was calculated on the basis of three measurements, each measurement consisting of six steps determining the amount of nitrogen adsorbed at six relative pressure points in the range of 0.05 to 0.3 of relative pressure, p/p_0, with an equilibration time of 10s.

Dissolution Studies under Sink Conditions

Dissolution studies under sink conditions were performed on a USP type IV flow-through dissolution apparatus (Sotax AG, Switzerland) with a 12 mm diameter cell in an open-loop configuration due to the very low solubility of ITR and POS [13]. The conical part of the cell was filled with glass beads of 1 mm diameter and a single ruby bead of approximately 5 mm diameter at the inlet. A filter head was composed, sequentially from bottom to top, of a cellulose Whatman filter grade 1 (11 µm), a Whatman GF/D 2.7 glass microfiber filter (Fisher Scientific, Dublin, Ireland), a Whatman GF/F 0.7µm glass microfiber filter and a hydrophilic membrane Pall Supor

(0.2 μm) and placed at the top of the cell to retain undissolved spheres. A pulsing flow of 4 ml/min was employed. Apparatus IV is proven to be useful in dissolution studies whereby a media change is required [13]. The study was performed for 1 hour in Fed-State Simulated Gastric Fluid (FaSSGF), following which the media was switched to Fasted-State Simulated Intestinal Fluid (FaSSIF) and the study was continued for another 4 hours. The pH of the filtrate was measured at predetermined intervals using a Thermo Orion 420+pH meter (Thermo Scientific, Hampshire, UK). The experiments were repeated at least in triplicate.

Atomic Force Microscopy (AFM) and Nanoscale Thermal Analysis (nanoTA)

The investigation of the microscopic texture and localized nanoscale thermal analysis of the spheres' remnants following dissolution studies was carried out using a nano-IR AFM-IR instrument (Anasys Instruments, Inc., Santa Barbara, CA, U.S.A.). AFM images were acquired in tapping mode using tapping mode AFM probes (Model: EXT125). Topographical images were collected using the Analysis Studio software (version 3.10.5539, Anasys Instruments, Inc., Santa Barbara, CA). For nanoTA measurements, temperature calibration was performed using three crystalline polymers with melting points covering the entire temperature range of interest. The polymers used were polycaprolactone ($T_{melting}$ = 55 °C), polyethylene ($T_{melting}$ = 116 °C), and polyethylene terephthalate ($T_{melting}$ = 235 °C). A ThermaLever™ probe (model EXP-AN2-200, Anasys Instruments Inc., Santa Barbara, CA) was used in intermittent contact mode. The probe was placed on the area of interest and the AFM tip was heated linearly with time, and the bending of the probe was recorded. The temperature at which a thermal event, defined as a penetration of the probe into the surface of the sample due to sample softening, occur is the glass transition for disordered substances and melting for crystalline materials.

Results and Discussions

Eudragit L100-55 (EUD) was chosen as the enteric polymer for this particular study due to its reported ability to maintain supersaturation of ITR for longer time compared to hypromellose phthalate (HP-55)[14]. The ratio of drug:polymer in the ASD was chosen based on data published by Overhoff et al. where a on phase "composite", depicted by a single T_g, was observed when the 1:2 w/w ratio of ITR to EUD was used[14].

Drug Content, Size and Morphology of the Spheres

The drug content in the coated beads was very similar and was 8.55 ± 0.31% and 8.42 ± 0.25% for the POS/EUD and ITR/EUD TAP-based formulations as well as 8.62 ± 0.17% and 8.34 ± 0.28% for the POS/EUD and ITR/EUD CEL-based formulations, respectively.

A comparison of the size of the coated and uncoated beads using laser diffraction is shown in Figure 2. The increase in d(0.1), d(0.5) and d(0.9) reflects the successful coating of both CEL and TAP spheres. The span, a measurement of the width of the size distribution, was 0.592±0.006 and 0.614±0.0005 for uncoated CEL and TAP, respectively and remained within 4% of these values upon coating. On the other hand, uniformity, a measure of the absolute deviation from the median particle size (d(0.5)), was 0.18, the same for CEL and TAP spheres, and remained the same after coating.

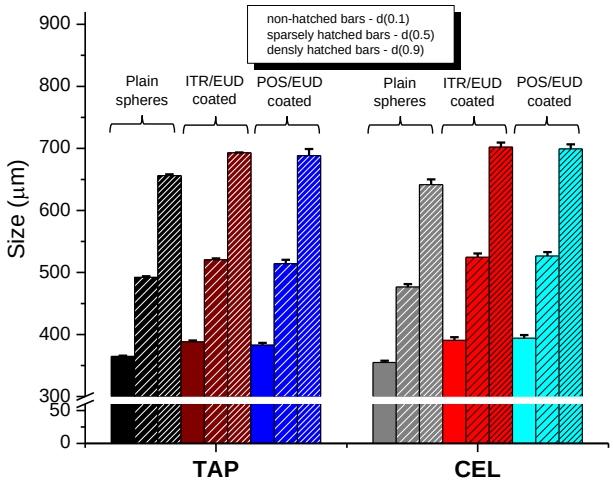

Figure 2. Values of d(0.1), d(0.5) and d(0.9) of the spheres before and after coating with ITR/EUD (1:2 w/w) and POS/EUD (1:2 w/w) solid dispersions.

Morphologies of the spheres before and after coating were examined using SEM. SE micrographs of the "as received" spheres illustrates rough surfaces of CEL and TAP beads (Figure 3). Surfaces of TAP spheres presented microcrystals of tartaric acid. Specific surface area values using BET were 0.0487±0.0026 m^2/g and 0.0455±0.0036 m^2/g for "as received" CEL and TAP, respectively. Following coating, surfaces of both types of spheres showed the presence of small, non-spherical irregular particles (Figure 4) described as morphology type 2 according to the classification system developed by Paluch et al[15]. These raisin-shaped particles are typical of cold/slow drying where the droplet temperature is below the boiling point of the solvent when the droplet skin formed[16]. This is consistent with the conditions used in our coating process, where the inlet gas temperature used was 40 °C. The solvents used in the coating process can form an azeotropic mixture with a boiling point of 39.85 °C at a DCM concentration of 95%[17]. At the ratio employed in this study, DCM is expected to evaporate first followed by ethanol.

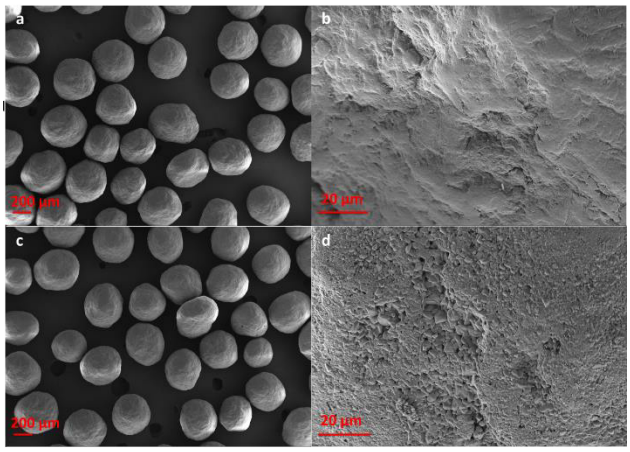

Figure 3. SE micrographs of (a), (b) CEL and (c), (d) TAP plain beads before coating.

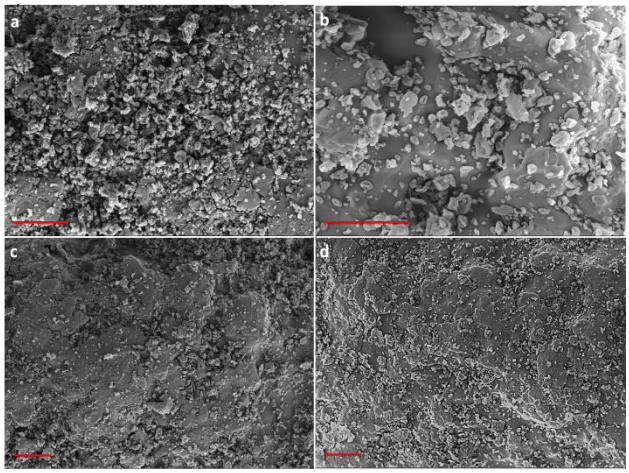

Figure 4. SE micrographs of the surface of (a) ITR/EUD and (b) POS/EUD coated TAP beads and (c) ITR/EUD and (d) POS/EUD coated CEL beads illustrating the morphology of the solid dispersion deposited on the surface of beads (the red bar represents 10 µm scale).

Evaluation of Solid-State Properties of ASD Coating

The solid-state properties of the material dried on the surface of TAP and CEL spheres were assessed using PXRD and DSC. X-ray diffractograms of the plain and drug-polymer coated beads revealed the absence of characteristic peaks of crystalline POS and ITR (Figure 5). In addition, the crystalline peaks of TAP and CEL substrates present in the diffractograms of coated breads were of lower intensities in comparison to their uncoated counterparts, which can be interpreted as the effect of the amorphous nature of the material coating the crystalline spheres.

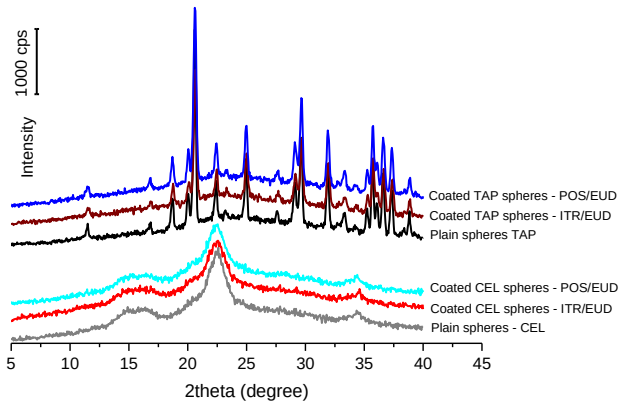

Figure 5. PXRD diffractograms of the plain TAP and CEL beads and their drug/polymer coated counterparts.

Modulated DSC (mDSC) was used to detect the glass transition (T_g) of the drug/EUD amorphous mixtures present at the surface of the spheres. The absence of a universally applicable sample preparation method for the DSC analysis of coated beads was addressed previously by Dereymaker and Van den Mooter[4]. Crushing followed by sieving has been reported to enable determination of the T_g of the solid dispersion deposited on sugar beads[4]. In an attempt to avoid such a pre-processing step, the T_{zero} aluminum pan was loaded with beads up to its maximum capacity. The T_gs of ITR, POS and EUD are 59, 59 and 128 °C, respectively [8,14,18]. Reversing heat flow, presented in Figure 6, indicates that all formulations exhibited a mid-point glass transition at 105-107 °C. This value correlates closely with the predicted value (102.7 °C) for these particular amorphous binary mixtures using the Gordon-Taylor equation, indicating the formation of a miscible binary amorphous solid dispersion on the surface of beads[14]. It should be highlighted that the dispersions deposited on TAP spheres, especially the POS dispersion, exhibited broader T_g events whereby a larger difference between T_g onset and offset values are observed indicating the possible instability of the ASD coat deposited on the TAP spheres[19]. This could be attributed to the presence of a possible competition between EUD and tartaric acid for interactions with the drugs since both of them are acidic in nature and potentially able to interact with the basic ITR and POS.

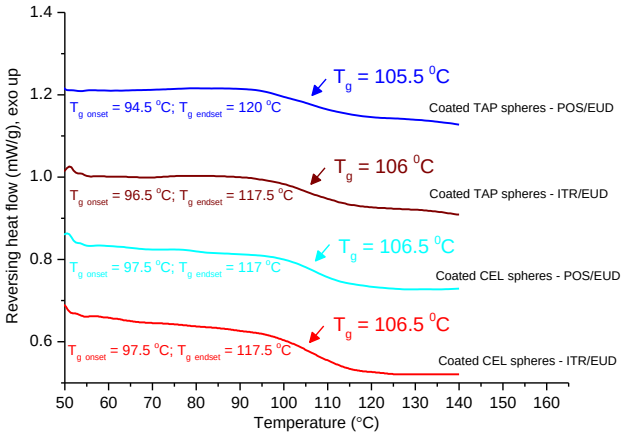

Figure 6. mDSC thermograms (reversing heat flow) of the solid dispersions present on the surface of coated TAP and CEL spheres indicating the composite glass transition temperature.

3.3 Evaluation of Polymer-Drug and Sphere-Drug Interactions

FTIR was utilized to investigate possible interactions between ITR or POS and the various components of the formulation.

FTIR spectra of the "as received" EUD, TAP and CEL beads, disordered (milled) ITZ (mITR), mITR physically mixed with crushed TAP beads in a mortar (1:7 w/w, PM mITR/TAP), mITR physically mixed with crushed CEL beads in a mortar (1:7 w/w, PM mITR/CEL) and ITR/EUD ASD (1:2 w/w), prepared via solvent evaporation, were analyzed. No changes were observed in the fingerprint region (below 1200 cm^{-1}) of mITR when physically mixed with crushed TAP or CEL spheres or in the ITR/EUD ASD. In contrast, some changes in the FTIR spectrum of ITR/EUD ASD were observed in the region 1450-1800 cm^{-1} as shown in Figure 7a. In the spectrum of mITR, the peak occurring at 1703 cm^{-1} is characteristic of a C=O stretching vibration. Absorptions at 1613, 1580 and 1553 cm^{-1} correspond to the stretching vibrations of C=C, C=N and C-N, while the peak observed at 1512 cm^{-1} could be assigned to the aromatic C=C vibration. The symmetric and asymmetric C-N stretching bands of the piperazine ring are usually challenging to identify, however they are expected to appear between 1199 and 1325 cm^{-1} [20]. On the other hand,

EUD exhibited a peak at 1734 cm^{-1} due to the carbonyl stretch of the carboxylic group. The carbonyl peak of ITR at 1703 cm^{-1} was masked by the carbonyl stretching of EUD and this could be due to the high EUD to ITR mass mixing ratio (2:1). However, it is clear that the shape of the carbonyl (of the carboxylic acid group) absorption region of EUD in the ITR/EUD ASD is different from that of the pure polymer. In addition, the carbonyl peak was slightly shifted in the spectrum of the ASD compared to the pure polymer, which could be due to the presence of a weak interaction between ITR and EUD in the ASD. Similarly, the absorption peaks at 1451, 1580 and 1613 cm^{-1} in mITR were shifted to 1454, 1584 and 1616 cm^{-1} in the ITR/EUD ASD. Overall, FTIR data suggests the presence of a weak interaction between ITR and EUD in the ASD with the possible interacting moieties being the carboxylic group of EUD and the piperazine and/or the triazole group of ITR. The latter has been reported before to participate in a hydrogen bond with the carboxylic acid of succinic acid to form an ITR:succinic acid co-crystal[21].

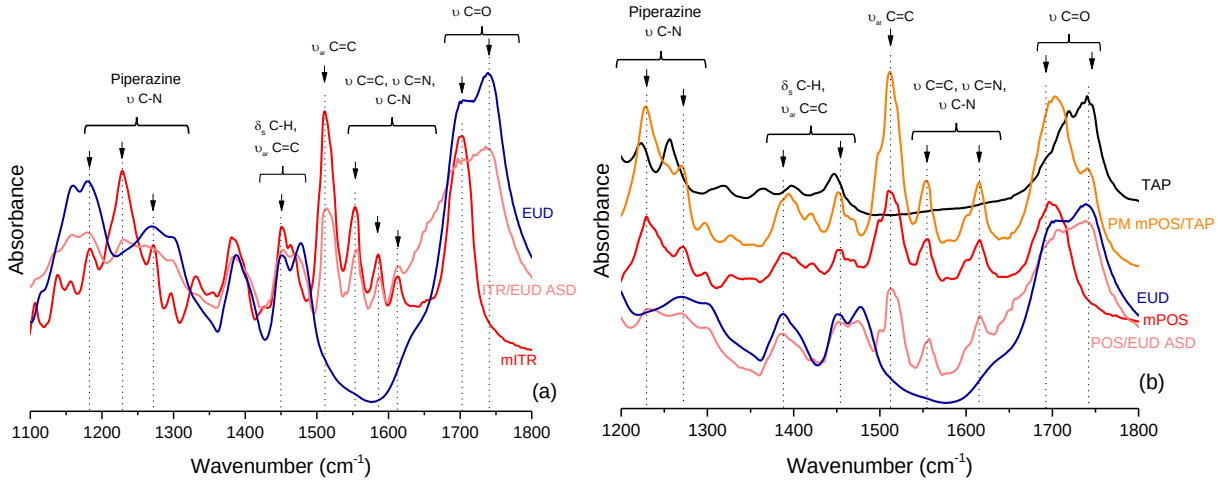

Figure 7. FTIR analysis of: (a) EUD "as received", milled ITR (mITR) and ITR/EUD ASD; (b) EUD "as received", TAP beads "as received", milled POS (mPOS), a physical mixture of mPOS and TAP beads and POS/EUD ASD. δ_s - in plane bending, υ - stretching.

In the case of POS, disordered (milled) POS (mPOS), mPOS physically mixed with crushed TAP beads in a mortar (1:7 w/w, PM mPOS/TAP), mPOS physically mixed with crushed CEL beads in

a mortar (1:7 w/w, PM mPOS/CEL) and POS/EUD ASD, prepared via solvent evaporation, were analyzed. The fingerprint region of mPOS did not show significant changes when physically mixed with CEL spheres. However, in the POS/EUD ASD sample, the =C-H out of plane bending band at 825 cm^{-1} showed a slight shift to 829 cm^{-1}. In addition, there were some changes in the aromatic bond stretching region (1350-1750 cm^{-1}) of POS in the PM mPOS/TAP sample. This region is displayed in Figure 7b. Similar to ITR, the peak at 1700 cm^{-1} in the spectrum of mPOS is characteristic of a C=O stretching vibration. Peaks at 1554 and 1620 cm^{-1} correspond to C=C, C=N and C-N stretching vibrations. The peak observed at 1510 cm^{-1} could be assigned to aromatic C=C bending, while the peaks of symmetric and asymmetric C-N stretching bands of the piperazine ring may appear in the region between 1200 and 1300 cm^{-1} [20]. As described above, EUD exhibited a peak at 1734 cm^{-1} due to the carboxylic group. In the PM mPOS/TAP sample, the carbonyl peak of POS was slightly blue shifted (1695 cm^{-1}) with respect to the peak observed for the carbonyl stretching in the mPOS sample (1700 cm^{-1}). Similarly, the peak at 1555 cm^{-1} was slightly red shifted to 1553 cm^{-1} compared to the mPOS sample, which could indicate the presence of weak interaction between POS and TAP. For the POS/EUD ASD produced via solvent evaporation, the carbonyl region between 1650 and 1750 cm^{-1} suggests the presence of a weak interaction between EUD and POS whereby the peak at 1555 cm^{-1} was shifted to 1558 cm^{-1}. Overall, FTIR data implies the presence of weak interactions between POS with both EUD and TAP, possibly between the carboxylic group of EUD and the piperazine group and/or triazole end of POS similar to what was observed for ITR, since both drugs possess similar chemical structures.

Interactions of Uncoated and Coated Spheres with Moisture at 25 °C

DVS studies, at 25 °C and up to 90% RH, on the spheres before and after coating are presented in Figures 8 and 9. Figure 8a illustrates the total water uptake for TAP spheres before and after

coating with ITR/EUD and POS/EUD ASDs. Plain TAP spheres exhibited a steep water sorption above 70% RH and gained more than 100% of its weight by the end of the sorption cycle. This could be explained by TAP deliquescence, as demonstrated using time-lapse imaging presented in Figure 8b. During desorption, a marked reduction in mass (14.8% w/w of the dry mass weight) was observed below 40% RH. This can be attributed to the efflorescence of the sample which was visible in the images taken throughout the analysis as displayed in Figure 8b. TAP spheres, coated with the ASDs, exhibited a delayed moisture sorption event starting at 80% RH with a lower amount of water sorbed by the end of the sorption cycle. Time-lapse imaging of POS/EUD coated TAP spheres, Figure 8c, indicates that the spheres retained their shape, which could be interpreted as a sign of successful coating of the spheres with the ASD. Notably, ITR/EUD coated TAP spheres sorbed less water (40% of its dry mass weight) compared to the POS/EUD coated TAP spheres (52% of its dry mass weight). This can be correlated with the higher water solubility of POS compared to ITR and the presence of a free –OH in POS, as shown in Figure 1, capable of forming H-bonds with water[22].

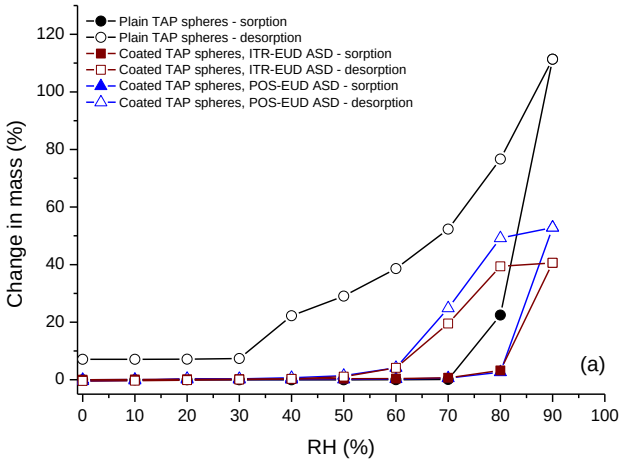

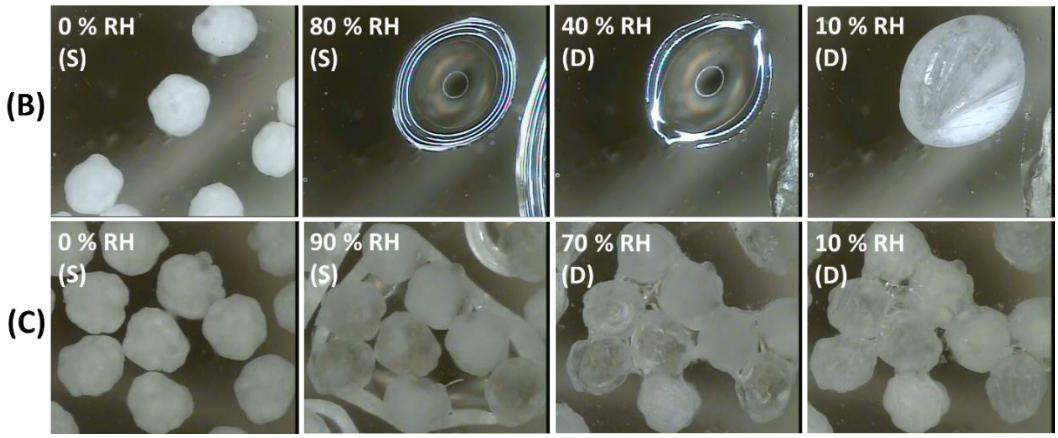

Figure 8. (a) DVS sorption-desorption profiles of plain, "as received" TAP spheres (circles), TAP spheres coated with POS/EUD (triangles) and ITR/EUD (squares) ASDs. (b) Optical images captured during the sorption (S) and desorption (D) cycles illustrating deliquescence and efflorescence of the TAP spheres. (c) Optical images captured during the sorption (S) and desorption (D) cycles illustrating interaction of the POS-EUD coated TAP spheres with moisture.

The "as received" CEL spheres sorbed a very small amount of water (9.6% of its dry mass weight) throughout the sorption cycle. Coating CEL spheres with ITR/EUD and POS/EUD ASDs resulted in the reduction in the amount of sorbed water to 7.8 and 8.2% of their dry mass weight, respectively. In addition, a hysteresis was observed in the isotherms of the "as received" and coated spheres, where the water content at each relative humidity step is higher during desorption than sorption[8,23]. It has been established that water is exclusively sorbed by the amorphous regions of MCC via tight attachment of a single water molecule per the anhydroglucose unit, followed by a second less tightly bound water molecule, with additional water sorbed in a more nonspecific manner. During exposure of cellulose to moisture, water molecules replace the cross-linking hydrogen bonds between cellulose chains and loosen the structure of cellulose until capillary condensation occurs. Because of the rough surface of uncoated and coated CEL beads, as demonstrated in Figures 3 and 4, water will condense into liquid in the pores by capillary condensation and water molecules will desorb at a lower relative humidity[23,24]. Collectively, DVS data suggests the permeability of both ITR and POS ASDs to water molecules.

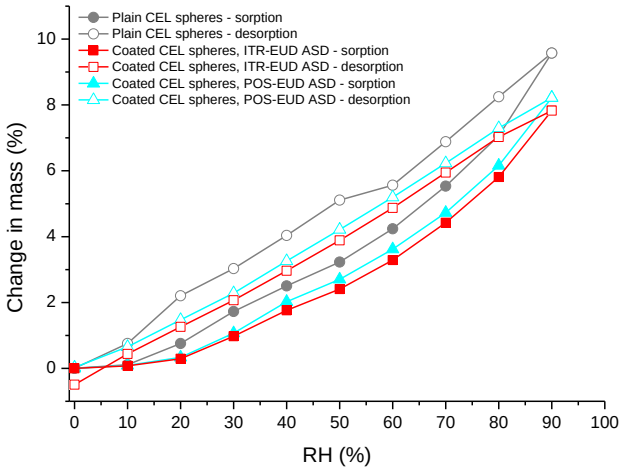

Figure 9. DVS sorption-desorption profiles of plain, "as received" CEL spheres (circles), CEL spheres coated with POS/EUD (triangles) and ITR/EUD (squares) ASDs.

Dissolution Studies of Coated TAP and CEL Beads

Dissolution apparatus IV was chosen herein due to its established advantages in testing the dissolution behavior of microspheres, especially when a media change during the experiment is required [13,25,26]. Figure 10 presents the dissolution profile of the four formulations (ITR/EUD TAP, ITR/EUD CEL, POS/EUD TAP and POS/EUD CEL) first subjected to 1 hr of dissolution in FaSSGF followed by a media change and dissolution in FaSSIF for 4 hr. The release of ITR in FaSSGF from the ITR/EUD CEL and ITR/EUD TAP formulations was negligible (less than 1%). Upon shifting the media to FaSSIF, both formulations started releasing the drug with the % ITR release from ITR/EUD CEL formulation always greater than that from ITR/EUD TAP. By the end of the dissolution study, 29% of ITR was released from ITR/EUD CEL formulation compared to 8% released from ITR/EUD TAP. This was counterintuitive due to the fact that tartaric acid is expected to create an acidic micro-environment in the vicinity of the ASD, which should improve ITR dissolution[8]. pH monitoring of the collected filtrate revealed reduction in the pH values recorded following pH shift in the case of the ITR/EUD coated TAP spheres.

To gain an insight into the dissolution process, a closer look at bead morphology during dissolution was undertaken using SEM as illustrated in Figure 11. SE micrographs of ITR/EUD TAP and ITR/EUD CEL removed from the dissolution medium at different stages are displayed in Figures 11a and b, respectively. After 1 hr in FaSSGF followed by 1 hr in FaSSIF, the surfaces of ITR/EUD coated TAP beads displayed very small, apparently crystalline structures embedded in the residual ASD matrix as shown in Figure 11a (left, inset). After additional 3 hr of dissolution in FaSSIF, needle-like shaped crystals, characteristic of ITR[10] were observed (Figure 11a, right). In contrast, there no crystallization was observed in the residual ITR/EUD CEL matrix following 1 hr dissolution in FaSSIF (Figure 11b, left, inset). Instead, spherical nano-species were observed; these were embedded in the ASD coat. The key question here was whether these nanoparticles were formed due to a phase separation of the ASD or deposited from the dissolution medium due to a phase separation in the liquid phase upon exceeding a certain supersaturation. An SE micrograph of the sample 1 hr later (Figure 11b, right) revealed the presence of more of these spherical nano-species and unlike those embedded in the coat observed after 1 hr, the nanoparticulates observed after 2 hr in FaSSIF were loosely attached to the surface. After 4 hr in FaSSIF, individual nanoparticles were observed on the MCC beads as illustrated by Figure 11b. This indicates that these nanoparticulates underwent phase separation from the ASD, then detached from the polymer matrix and became dispersed in the medium. It is noteworthy that upon fitting the cumulative release data following the media shift, ITR release from the ITR/EUD CEL formulation followed a linear (zero order) release profile with an adjusted R^2 of 0.9999, while an exponential ITR release was observed for the ITR/EUD TAP formulation.

Unfortunately, SEM is not able to provide information on the solid-state of the sample. To achieve this, an AFM coupled with a nanoTA was utilized (Figure 12). In general, it is challenging to

investigate non-flat surfaces using AFM[27]. Topographical images of the coat remaining at the end of dissolution studies (1 hr of FaSSGF followed by 4 hr of FaSSIF) of ITR/EUD TAP and ITR/EUD CEL formulations produced using tapping mode are displayed in Figures 12a and b. These morphologies are in agreement with those observed using SEM (Figure 11). Localized thermal analysis of the ITR/EUD CEL remnants collected from the dissolution medium after 1 and 2 hr of dissolution in FaSSIF is shown in Figure 12c and d, respectively. Softening temperatures, representative of T_g events, of the spherical domains observed in the ASD matrix in Figure 12c indicate that they are ITR domains. Notably, one of the investigated domains exhibited a slightly higher T_g (~76 °C) than that of pure ITR (59 °C[8,28]), which could be attributed to the presence of residual EUD. On the other hand, the T_gs of the remaining matrix suggest that this matrix is polymer-rich. Thermal investigation of the spheres 1 hr later (in total exposed to 1 hr in FaSSGF and 2 hr in FaSSIF) confirmed the glassy nature of the nanosized ITR spherical domains. For the ITR/EUD TAP spheres, the thermal investigation of the remnant after 1 hr in FaSSIF is displayed in Figure 12e. The thermal event recorded is in close agreement with the melting temperature of ITR. The slight melting point depression observed using nanoTA can be attributed to the presence of polymer residue[29] on ITR crystals, which indicates that ITR crystallized in the matrix.

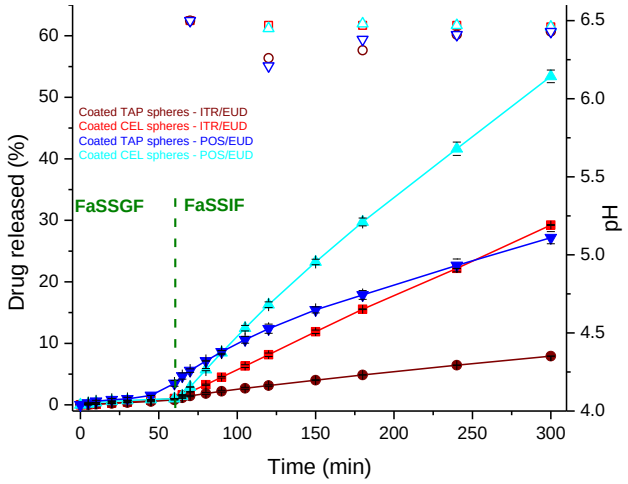

Figure 10. Cumulative drug release profiles (closed symbols) and the recorded pH of the filtrate (open symbols) for ITR released from ITR/EUD CEL (squares) and ITR/EUD TAP spheres (circles) as well as POS released from POS/EUD CEL spheres (triangles) coated with POS/EUD TAP (inverted triangles) using the open-loop configuration of USP IV flow through cell dissolution apparatus.

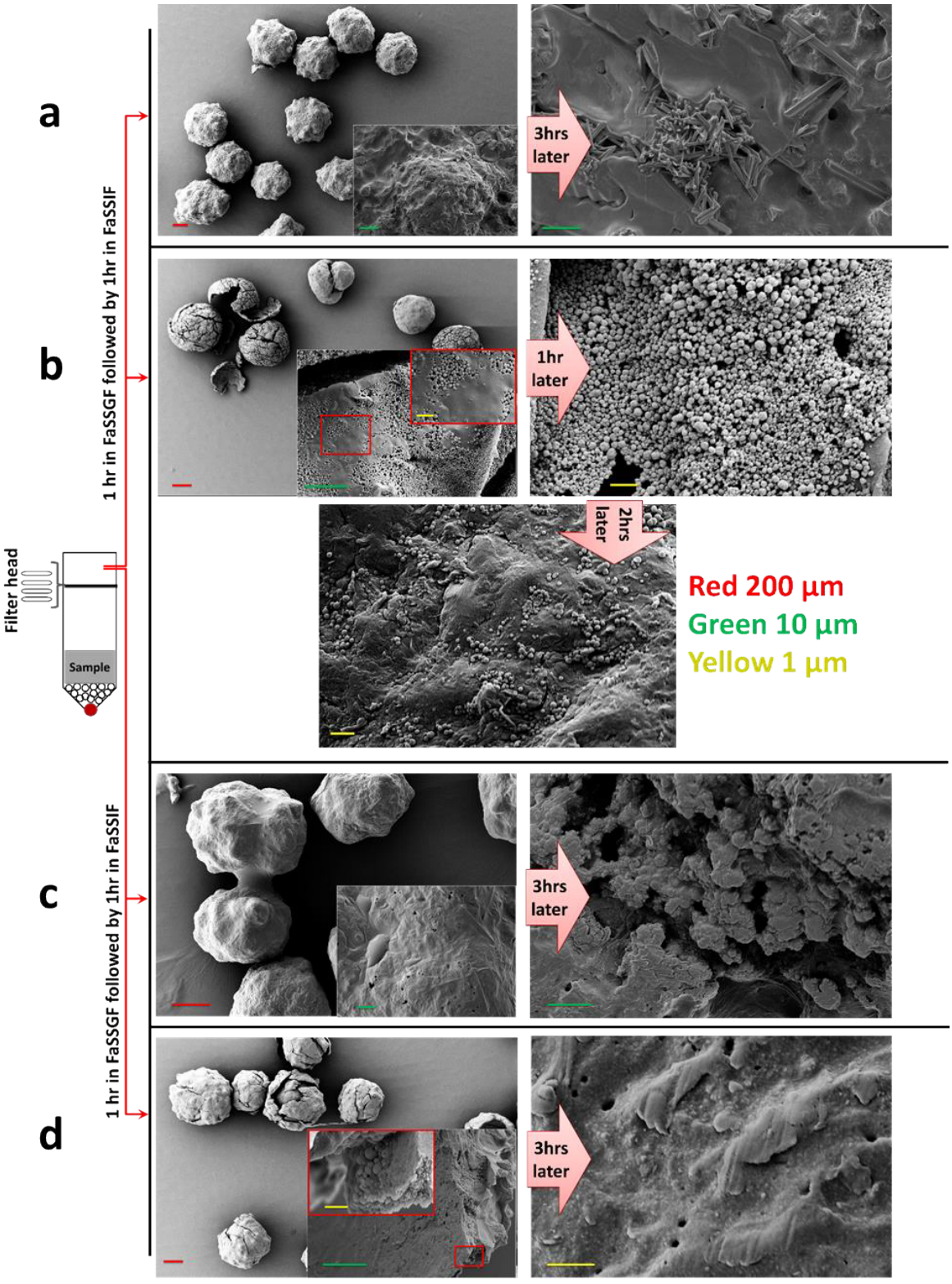

Figure 11. SE micrographs of (a) ITR/EUD TAP, (b) ITR/EUD CEL, (c) POS/EUD TAP and (d) POS/EUD CEL following dissolution for 1 hr in FaSSGF followed by 3 hr in FaSSIF using a USP

IV flow through cell dissolution apparatus (red, green and yellow bars represent 200, 10 and 1 µm scale, respectively).

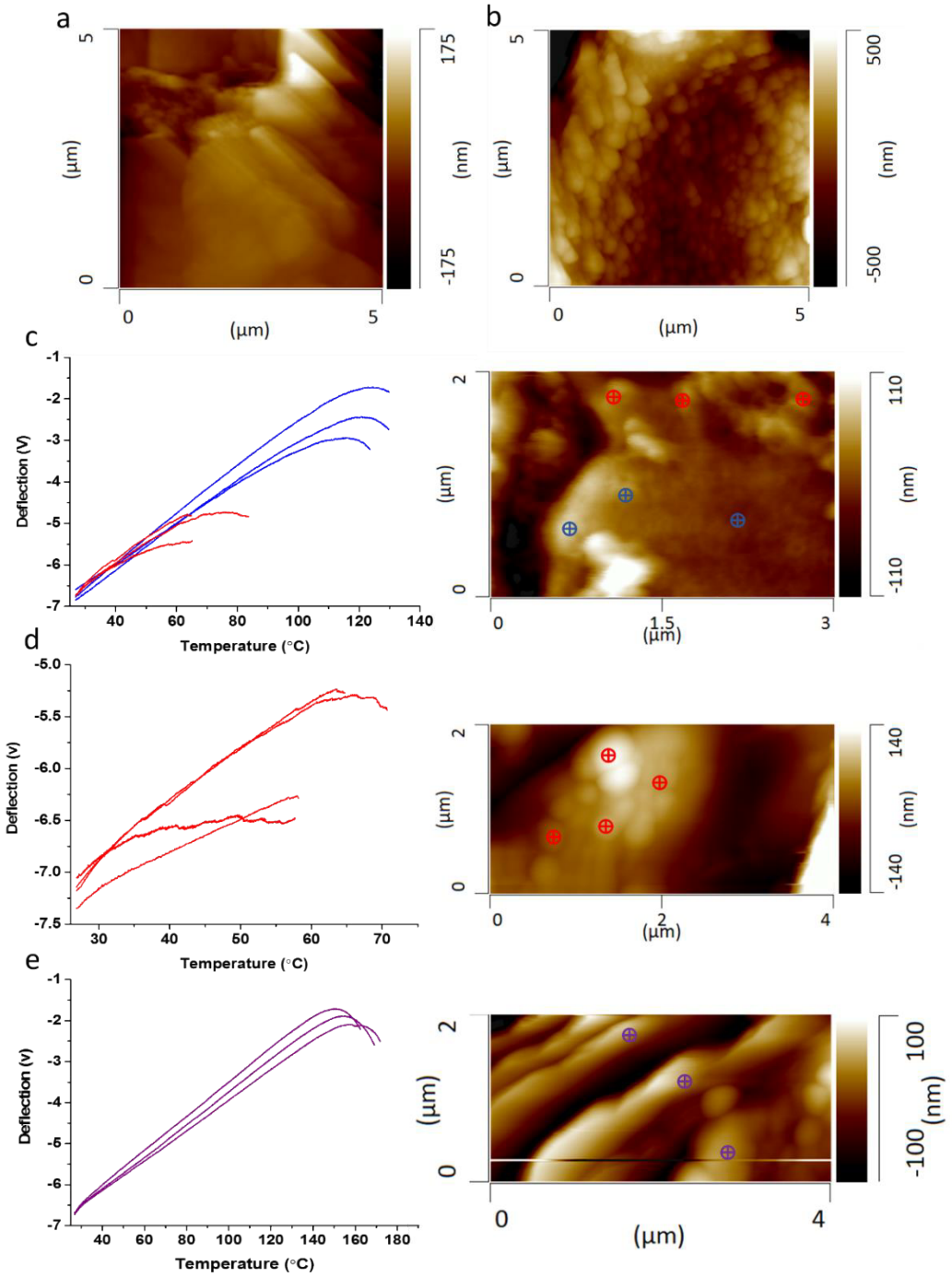

Figure 12. (a) and (b) AFM topographical images of ITR/EUD TAP and ITR/EUD CEL spheres, respectively, following dissolution testing for 1 hr in FaSSGF followed by 4 hr in FaSSIF and nanoTA and topographical images of (c) ITR/EUD CEL after 1 hr in FaSSGF followed by 1 hr in FaSSIF, (d) ITR/EUD CEL after 1 hr in FaSSGF followed by 2 hr in FaSSIF and (e) ITR/EUD TAP after 1 hr in FaSSGF followed by 1 hr in FaSSIF. The dip in the curve in the deflection versus

temperature plot represents the T_g of ITZ (red line), T_g of EUD (blue line) and $T_{melting}$ of ITZ (purple line).

POS release from the POS/EUD CEL formulation in FaSSGF was negligible (less than 1%). In contrast, there was approximately 3.6% release of POS from the POS/EUD TAP formulation after 60 min in FaSSGF. This indicates that EUD was not efficient in protecting the drug in the POS/EUD ASD coat deposited on TAP spheres from releasing in the acidic media. Upon shifting the dissolution media to FaSSIF, POS release began from POS/EUD CEL beads with 8.5% of POS released after 20 minutes in FaSSIF. On the other hand, POS release from the POS/EUD TAP formulation continued linearly for the first 20 min in FaSSIF before it started to slow down after 30 min in this medium, in comparison to the POS/EUD CEL system. At the end of the dissolution study, POS cumulative release from POS/EUD CEL (53±1%) was twice than that released from POS/EUD TAP (27±1%). pH monitoring of the collected filtrate revealed reduction in the pH values recorded following pH shift in the case of the POS/EUD coated TAP spheres. SEM data, Figures 11 c and d, acquired from the remnant of spheres were in line with the dissolution profiles. After 1 hr in FaSSIF, Figure 11 c (left, inset), the surface of POS/EUD coated TAP spheres displayed needle-like crystals embedded in the matrix. After additional 3 hr of dissolution in FaSSIF, small crystals were observed in the matrix as well (Figure 11c, right). In the case of POS/EUD coated CEL spheres, spherical nano-species were observed following 1 hr in FaSSIF similar to those observed in the ITR/EUD coated CEL spheres (Figure 11d, left, inset). After the total 4 hr of dissolution in FaSSIF, crystallization was observed in the matrix remnant as shown in Figure 11d (right).

Discussion

ASDs of ITR/EUD and POS/EUD were successfully coated on two different types of spheres made of tartaric acid (TAP) and microcrystalline cellulose (CEL). Both types of spheres exhibited

similar particle sizes and similar surface areas before coating. An increase of around 10% in the spheres' diameter was observed following coating, which corresponds to the thickness of the coat deposited on the spheres during the process. Morphological investigation revealed the presence of raisin-like particulates, similar to those typically obtained from cold/slow spray drying processes, on the surface of the spheres of all formulations. It should be highlighted that in the fluid bed coating process, high inlet temperatures are usually avoided to prevent rapid drying of the sprayed mist before reaching the spheres' surface[30]. The solid-state of polymeric coats was probed using PXRD and DSC. The latter suggested the formation of a single composite ASD on the surface of the spheres in case of all the four formulations with a possible competitive interaction between the drug and the polymer and the drug and tartaric acid in the TAP spheres. FTIR investigation of the interactions between the drug and EUD and between each type of the spheres and the drug suggested the presence of an interaction between ITR and EUD and POS and EUD, which could be attributed to the basic nature of the triazole antifungals and the acidic nature of the polymer. In addition, FTIR indicated that POS may possibly interact with TAP, but no such interaction was detected for the ITR and TAP mixture. This could be attributed to the fact that ITR is a weaker base and a more poorly soluble compound in comparison to POS and thus it is less likely that ITR will interact with weak acids such as tartaric acid[31]. To confirm the absence or presence such weak interactions, further studies involving solid state nuclear magnetic resonance and/or dielectric spectroscopy should be performed[32,33]. The presence of weak interactions between ITR or POS and EUD as well as single glass transition events detected for each of the mixtures suggest miscibility of the components in the blends deposited on the spheres. The marked reduction in the % of moisture sorbed by the coated spheres supports the successful and uniform deposition of the ASDs, also supported by the laser diffraction particle size measurements.

Dissolution studies performed in a USP IV flow through cell dissolution apparatus (open loop configuration, assumed to create sink conditions[13]) indicated the presence of different dissolution behavior of ASDs deposited on the different sphere types. A premature release of POS was observed from the POS/EUD TAP system in FaSSGF, possibly due to the competing interaction of POS with TAP. POS is a slightly stronger base than ITR, thus it dissolves quicker in acidic media. Upon media shift to FaSSIF, the POS release rate was reduced due to drug crystallization. Notably, unlike the POS/EUD CEL formulation, the polymer matrix (ASD coat) in the POS/EUD TAP system did not dissolve in FaSSIF. pH monitoring of the collected filtrate over the course of the dissolution study revealed a decrease in pH for both TAP formulations (ITR/EUD TAP and POS/EUD TAP) following 1 hr of dissolution in FaSSIF. This could explain the failure of EUD to dissolve in FaSSIF in the case of TAP formulations. Tartaric acid is expected to reduce pH in the microenvironment of EUD and thus prevent its solubilization given than this enteric polymer dissolves at pH higher than 5.5[34]. Towards the end of the dissolution study, more needle-shaped crystals were observed in the polymer matrix, which is consistent with the low percentage of released drug. The use of CEL appears to result in a phase separation of the ASD, due to hydration, leading to the formation of drug-rich nanospecies owing to the solubility gap between the drug and EUD in FaSSIF, where EUD dissolves faster following the media shift, confirmed by AFM/nanoTA data. Notably, some crystals were observed in the POS/EUD CEL formulation at the end of the dissolution experiment. In contrast, no crystallization was observed in the ITR/EUD CEL formulation. This can be attributed to the tendency of ITR to form nanosized liquid crystal (LC) assemblies in aqueous media[8,35]. The LC assembly of ITR has been reported to be resilient to full crystallization in aqueous environments[28]. The origin of nanospecies during dissolution is an ongoing topic of discussion in the area of ASDs. Two different mechanisms have been proposed

to date for dissolution-induced nanoparticle formation [36,37]. Mechanism I suggests that the polymer controls dissolution of the ASD and drives the drug associated with it into the liquid medium and, when the drug concentration exceeds amorphous solubility, a liquid-liquid phase separation and subsequent nanospecies formation takes place[36]. In contrast, Mechanism II suggests that the formation of dissolution-induced nanoparticle is due to a rapid amorphous drug domain formation within the ASD matrix[37]. Herein, it was clear that the dissolution-induced nanoparticles were produced through Mechanism II. It should be highlighted that both mechanisms were proposed based on dissolution studies carried out under supersaturation conditions while our study employed a USP apparatus IV with an open-loop configuration, where a fresh media purges the sample throughout the study to maintain sink conditions. To the best of our knowledge, the formation of dissolution-induced nanoparticulates during dissolution testing using a similar set-up has not been reported before. Dissolution-induced drug nano-species have been reported to act as a drug reservoir, replenishing absorbed drug and thus maintaining supersaturation at a constant value during absorption given that crystallization is avoided[38]. This is in line with the zero order release observed from the ITR/EUD ASD coated on CEL spheres where the dissolution-induced nano-species did not crystalize throughout the dissolution experiment.

Conclusions

The fluid bed coating of ITR and POS solid dispersions with EUD on tartaric acid and microcrystalline cellulose based spheres was achieved. An investigation into the impact of the type of nonpareil spheres coated with ITR and POS ASDs produced using fluid bed coating revealed that, unlike neutral spheres, spheres made of acidic components produced miscible ASD with compositional variations. During dissolution studies, TAP spheres created a microenvironment with low pH which hindered the release of basic drugs from the ASDs. This resulted in dissolution

induced crystallization and poor release profile. A dissolution-induced phase separation into nanoparticles was observed when the ASDs were coated on neutral MCC spheres. Depending on the drug properties those nanoparticles can undergo crystallization, such as in the POS case, or remain in the dissolution media to replenish the dissolved drug such as in the ITR case.

Author Information

Corresponding Author

*Phone: +35318962787, email: ltajber@tcd.ie.

Acknowledgements

This work was funded by the Libyan embassy in London and Science Foundation Ireland under grant No. 12/RC/2275 (Synthesis and Solid State Pharmaceutical Centre). AFM and nanoTA experiments carried out at Purdue University (IN, USA) were funded by the U.S Food and Drug Administration (FDA) through the National Institute for Pharmaceutical Technology and Education (NIPTE). The Pharmaceutical Research and Manufacturers of America (PhRMA) Foundation is acknowledged for a post-doctoral fellowship granted to NM. The authors would like to thank Fredy Hettlinger (Pharmatrans Sanaq AG, Switzerland) for kindly supplying the beads and Dr. Deirdre Darcy for providing access to the US apparatus IV.

Notes

The authors declare no competing financial interest.

References

(1) Bodmeier, R. Tableting of coated pellets. *Eur. J. Pharm. Biopharm.* **1997,** *43,* 1-8.

(2) Bechgaard, H.; Nielson, GH. Controlled release multiple units and single-unit doses. *Drug Dev. Ind. Pharm.* **1978,** *4*, 53-67.

(3) Bechgaard, H.; Ladefoged, K. Distribution of pellets in the gastrointestinal tract. The influence on transit time exerted by the density or diameter of pellets. *J. Pharm. Pharmacol.* **1978,** *30*, 690-692.

(4) Dereymaker, A.; Van Den Mooter, G. The peculiar behavior of the glass transition temperature of amorphous drug-polymer films coated on inert sugar spheres. *J. Pharm. Sci.* **2015,** *104*, 1759-1766.

(5) Serajuddin, A. T. Solid dispersion of poorly water-soluble drugs: early promises, subsequent problems, and recent breakthroughs. *J. Pharm. Sci.* **1999,** *88*, 1058-1066.

(6) Zhang, J.; Bunker, M.; Parker, A.; Madden-Smith, C. E.; Patel, N.; Roberts, C. J. The stability of solid dispersions of felodipine in polyvinylpyrrolidone characterized by nanothermal analysis. *Int. J. Pharm.* **2011,** *414*, 210-207.

(7) Purohit, H. S.; Taylor, L. S. Miscibility of Itraconazole-Hydroxypropyl Methylcellulose Blends: Insights with High Resolution Analytical Methodologies. *Mol. Pharm.* **2015,** 12, 4542-4553.

(8) Mugheirbi, N. A.; Paluch, K. J.; Tajber, L. Heat induced evaporative antisolvent nanoprecipitation (HIEAN) of itraconazole. *Int. J. Pharm.* **2014,** *471*, 400-11.

(9) Barrett, A. M.; Dehghani, F.; Foster, N. R. Increasing the dissolution rate of itraconazole processed by gas antisolvent techniques using polyethylene glycol as a carrier. *Pharm. Res.* **2008,** *25*, 1274-1289.

(10) Mugheirbi, N. A.; Tajber, L. Crystal Habits of Itraconazole Microcrystals: Unusual Isomorphic Intergrowths Induced via Tuning Recrystallization Conditions. *Mol. Pharm.* **2015,** *12*, 3468-3478.

(11) Moton, A.; Ma, L.; Krishna, G.; Martinho, M.; Seiberling, M.; McLeod, J. Effects of oral posaconazole on the pharmacokinetics of sirolimus. *Curr. Med. Res. Opin.* **2009,** 25, 701-707.

(12) Percival, K. M.; Bergman, S. J. Update on Posaconazole Pharmacokinetics: Comparison of Old and New Formulations. *Curr. Fungal Infect. Rep.* **2014,** *8*, 139-145.

(13) Fotaki, N. Flow-Through Cell Apparatus (USP Apparatus 4): Operation and Features. *Dissolut. Technol.* **2011,** *18*, 46-49.

(14) Overhoff, K. A.; Moreno, A.; Miller, D. A.; Johnston, K. P.; Williams, R. O., 3rd Solid dispersions of itraconazole and enteric polymers made by ultra-rapid freezing. *Int. J. Pharm.* **2007,** *336*, 122-132.

(15) Paluch, K. J.; Tajber, L.; Corrigan, O. I.; Healy, A. M. Impact of process variables on the micromeritic and physicochemical properties of spray-dried porous microparticles, part I: introduction of a new morphology classification system. *J. Pharm. Pharmacol.* **2012,** *64*, 1570-1582.

(16) Dobry, D. E.; Settell, D. M.; Baumann, J. M.; Ray, R. J.; Graham, L. J.; Beyerinck, R. A. A Model-Based Methodology for Spray-Drying Process Development. *J. Pharm. Innov.* **2009,** *4*, 133-142.

(17) Baird, J. K. Primaquine toxicity forestalls effective therapeutic management of the endemic malarias. *Int. J. Parasitol.* **2012,** *42*, 1049-1054.

(18) Adrjanowicz, K.; Kaminski, K.; Wlodarczyk, P.; Grzybowska, K.; Tarnacka, M.; Zakowiecki, D.; Garbacz, G.; Paluch, M.; Jurga, S. Molecular dynamics of the supercooled pharmaceutical agent posaconazole studied via differential scanning calorimetry and dielectric and mechanical spectroscopies. *Mol Pharm*. **2013**, *10*, 3934-3945.

(19) Lipson, J. E. G.; Milner, S. T. Multiple glass transitions and local composition effects on polymer solvent mixtures. *J. Polym. Sci. Part B Polym. Phys.* **2006,** *44*, 3528–3545.

(20) Gunasekaran, S.; Anita, B. Spectral investigation and normal coordinate analysis of piperazine. *Indian J. Pure Appl. Phys*. **2008**, *46*, 833-838.

(21) Lahtinen, M.; Kolehmainen, E.; Haarala, J.; Shevchenko, A. Evidence of Weak Halogen Bonding: New Insights on Itraconazole and its Succinic Acid Cocrystal. *Cryst. Growth Des.* **2013,** *13*, 346-351.

(22) Fang, L. Y.; Harris, D.; Krishna, G.; Moton, A.E.; Prestipino, R.C.; Steinman, M.; Wan, J.; Waskin, H.A. Oral pharmaceutical compositions in a solid dispersion comprising preferably posaconazole and HPMCAS. **2011**, US20110034478 A1.

(23) Airaksinen, S.; Karjalainen, M.; Shevchenko, A.; Westermarck, S.; Leppanen, E.; Rantanen, J.; Yliruusi, J. Role of water in the physical stability of solid dosage formulations. *J. Pharm. Sci.* **2005,** *94*, 2147-2165.

(24) Zografi, G. D; Kontny M. J.; Yang A.Y.; Brenner G.S. Surface area and water vapour sorption of microcrystalline cellulose. *Int. J. Pharm.* **1984,** *18*, 99-116.

(25) Zolnik, B.S.; Raton J.-L.; Burgess D. J. Application of USP apparatus 4 and in situ fiber optic analysis to microsphere release testing. *Dissolut. Technol.* **2005,** *12*, 11-14.

(26) Zolnik, B. S.; Burgess, D. J. Effect of acidic pH on PLGA microsphere degradation and release. *J. Control. Release* **2007,** *122*, 338-344.

(27) Burson, K. M.; Yamamoto, M.; Cullen, W. G. Modeling noncontact atomic force microscopy resolution on corrugated surfaces. *Beilstein J. Nanotechnol.* **2012,** *3*, 230-237.

(28) Mugheirbi, N. A.; Fleischer, K.; Tajber, L. A Rare Case of Mesomorphic Behavior-Molecular Reorientation of Itraconazole Liquid Crystal Induced by a Hygrothermal Treatment. *Cryst. Growth Des.* **2016,** *16*, 1329-1336.

(29) Marsac, P. J.; Li, T.; Taylor, L. S. Estimation of drug-polymer miscibility and solubility in amorphous solid dispersions using experimentally determined interaction parameters. *Pharm. Res.* **2009,** *26*, 139-151.

(30) Farag, Y.; Leopold, C. S. Influence of the inlet air temperature in a fluid bed coating process on drug release from shellac-coated pellets. *Drug Dev. Ind. Pharm.* **2011,** *37*, 320-328.

(31) Courtney, R. W. D.; Radwanski, E.; Lim, J.; Laughlin, M. Effect of food on the relative bioavailability of two oral formulations of posaconazole in healthy adults. *Br. J. Clin. Pharmacol.* **2004,** *57*, 218-222.

(32) Mistry, P.; Mohapatra, S.; Gopinath, T.; Vogt, F. G.; Suryanarayanan, R. Role of the Strength of Drug-Polymer Interactions on the Molecular Mobility and Crystallization Inhibition in Ketoconazole Solid Dispersions. Mol Pharm. **2015**, *12*, 3339-3350.

(33) Nie, H.; Su, Y.; Zhang, M.; Song, Y.; Leone, A.; Taylor, L. S.; Marsac, P. J.; Li, T.; Byrn, S. R. Solid-State Spectroscopic Investigation of Molecular Interactions between Clofazimine and Hypromellose Phthalate in Amorphous Solid Dispersions. Mol Pharm. **2016**, *13*, 3964-3975.

(34) Jelvehgari, M.; Zakeri-Milani, P.; Siahi-Shadbad, M. R.; Loveymi, B. D.; Nokhodchi, A.; Azari, Z.; Valizadeh, H. Development of pH-sensitive insulin nanoparticles using Eudragit L100-55 and chitosan with different molecular weights. *AAPS PharmSciTech.* **2010,** *11*, 1237-1242.

(35) Mugheirbi, N. A.; Tajber, L. Mesophase and size manipulation of itraconazole liquid crystalline nanoparticles produced via quasi nanoemulsion precipitation. *Eur. J. Pharm. Biopharm.* **2015,** *96*, 226-236.

(36) Indulkar, A. S.; Waters, J. E.; Mo, H.; Gao, Y.; Raina, S. A.; Zhang, G. G. Z.; Taylor, L. S. Origin of Nanodroplet Formation upon Dissolution of an Amorphous Solid Dispersion: A Mechanistic Isotope Scrambling Study. *J. Pharm. Sci.* **2017,** doi: 10.1016/j.xphs.2017.04.015.

(37) Harmon, P.; Galipeau, K.; Xu, W.; Brown, C.; Wuelfing, W. P. Mechanism of Dissolution-Induced Nanoparticle Formation from a Copovidone-Based Amorphous Solid Dispersion. *Mol. Pharm.* **2016,** *13*, 1467-1481.

(38) Raina, S. A.; Zhang, G. G. Z.; Alonzo, D. E.; Wu, J. W.; Zhu, D. H.; Catron, N. D.; Gao, Y.; Taylor, L. S. Enhancements and Limits in Drug Membrane Transport Using Supersaturated Solutions of Poorly Water Soluble Drugs. *J. Pharm. Sci.* **2014,** *103*, 2736-2748.

For Table of Contents Use Only

A comparative study on the performance of inert and functionalized spheres coated with solid dispersions made of two structurally related antifungal drugs

Naila A. Mugheirbi, Peter O'Connell, Dolores R. Serrano, Anne Marie Healy, Lynne S. Taylor and Lidia Tajber